

**Amino-Fulleropyrrolidines as Electrotropic Additives to  
Enhance Organic Photovoltaics**

Journal:	<i>Sustainable Energy &amp; Fuels</i>
Manuscript ID	SE-COM-06-2018-000294.R1
Article Type:	Communication
Date Submitted by the Author:	22-Jul-2018
Complete List of Authors:	Karak, Supravat; Nagoya Daigaku Kogakubu Daigakuin Kogaku Kenkyuka, Page, Zachariah; University of California, Materials Research Laboratory Li, Shaoguang; University of California Santa Barbara Tinkham, Jonathan; Colorado School of Mines, Chemistry Lahti, Paul; University of Massachusetts, Department of Chemistry Duzhko, Volodimir; University of Massachusetts-Amherst, Department of Polymer Science and Engineering Emrick, Todd; University of Massachusetts-Amherst, Polymer Science and Engineering



# Sustainable Energy & Fuels

## COMMUNICATION

### Amino-Fulleropyrrolidines as Electrotropic Additives to Enhance Organic Photovoltaics

Received 00th January 20xx,  
Accepted 00th January 20xx

Supravat Karak,<sup>a†</sup> Zachariah A. Page,<sup>\*a†</sup> Shaoguang Li,<sup>b†</sup> Jonathan S. Tinkham,<sup>c§</sup> Paul M. Lahti,<sup>c</sup>  
Volodymyr V. Duzhko,<sup>a</sup> and Todd Emrick<sup>\*a</sup>

DOI: 10.1039/x0xx00000x

www.rsc.org/

**The synthesis, device fabrication, and electric poling of novel amino-functionalized fulleropyrrolidines in polymer solar cells is reported. Systematically varying the tether lengths between the fullerene cage and tertiary amines provides insight into enhanced device efficiency and stability after poling. DFT calculations in an external electric field results in alignment of molecular dipole moments, which corroborates our hypothesis that electrotropic polarization causes an increased built-in electrostatic potential difference across the device, and results in enhance performance.**

Organic polymer solar cells (OPSCs) are regarded as inexpensive, flexible, and light-weight sources of energy, where ease of solution processability, abundance of raw starting materials, and mechanical integrity make them particularly attractive. Small amounts of additives to bulk-heterojunction (BHJ) active layers has led to significant advances in OPSC technology, by improving device performance and stability. For example, compatibilizers<sup>1–5</sup> have been used to prevent phase-segregation to improve device lifetimes, while low vapor pressure solvents (e.g., 1,8-diiodooctane) modify the BHJ morphology and increase power conversion efficiency (PCE)<sup>6–8</sup>. Alternatively, dipolar additives that reorient in response to an applied electric field (i.e., electrotropic compounds) were recently shown to improve PCE values of standard-geometry solar cells (e.g., anode to cathode from bottom up) with small molecule-based BHJs, due to an increased electrostatic potential difference across the device.<sup>9</sup> To better understand and utilize electrotropic

materials in photovoltaic technology, a more systematic study between structure and function of dipolar additives in BHJ active layers is critical.

Dipolar materials have found utility as interlayers in OPSCs to elicit significant improvements in device performance, which, in-part, stems from the increase in built-in electrostatic potential across the device.<sup>10–22</sup> Numerous examples of tertiary amine-functionalized materials have recently been developed and employed as efficient electrode work function modifiers through their use as interlayers. The proposed operational mechanisms for tertiary amines include the alignment of dipolar side-chains for p-type<sup>10</sup> or insulating<sup>11</sup> polymer backbones, doping of the acceptor component in the adjacent active layer,<sup>23</sup> and self-doping of n-type polymers.<sup>12,17</sup> Recently, we demonstrated that a tertiary amine-functionalized fulleropyrrolidine (C<sub>60</sub>-N-T<sub>3</sub>) is susceptible to ferroelectric polarization.<sup>9</sup> Specifically, integration of C<sub>60</sub>-N-T<sub>3</sub> into a small molecule BHJ active layer followed by electric field poling led to a significant improvement in device performance, which was largely attributed to the electric-field induced alignment of dipolar side groups, which increases the overall built-in potential difference across the device active layer. However, to-date electrotropism in OPSCs has only been shown with this one dipolar additive (C<sub>60</sub>-N-T<sub>3</sub>) and in one type of device configuration (standard geometry, small molecule BHJ).

To understand the versatility of electrotropism in solar cells, two new amine-functionalized fulleropyrrolidine derivatives, C<sub>60</sub>-N-T<sub>6</sub> and C<sub>60</sub>-N-T<sub>11</sub>, with different tether lengths connecting the tertiary amines and fullerene core, were synthesized, and together with C<sub>60</sub>-N-T<sub>3</sub>, were studied as additives in inverted polymer-based solar cells. The effect of tether length on ferroelectric polarization was probed by testing device metrics over time. Additionally, density functional theory (DFT) calculations on the additives in the presence and absence of an external electric field was used to correlate chemical structure to device metrics.

<sup>a</sup>Department of Polymer Science and Engineering, University of Massachusetts, Amherst, Massachusetts 01003, USA. E-mail: zapage@mrl.ucsb.edu; tsemrick@mail.pse.umass.edu

<sup>b</sup>Materials Research Lab, University of California, Santa Barbara, CA 93106, USA  
<sup>c</sup>Department of Chemistry, University of Massachusetts, Amherst, Massachusetts 01003, USA

<sup>†</sup>Present address: Centre for Energy Studies, Indian Institute of Technology, Delhi, Hauz Khas New Delhi - 110016, India

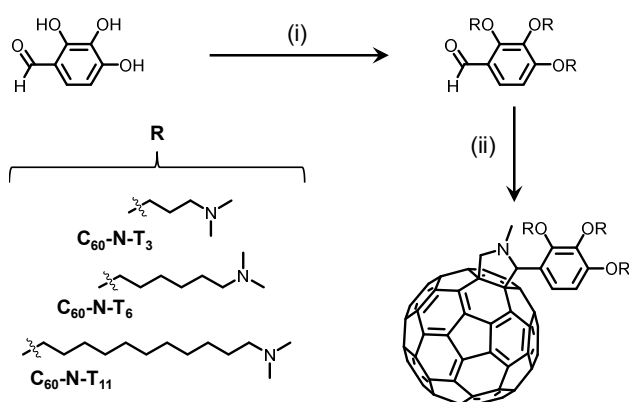
<sup>‡</sup>Present address: Materials Research Lab, University of California, Santa Barbara, CA 93106, USA

<sup>§</sup>Present address: Department of Chemistry and Geochemistry, Colorado School of Mines, Golden, CO 80401, USA

Electronic Supplementary Information (ESI) available: Synthetic details and additional device testing. See DOI: 10.1039/x0xx00000x

## COMMUNICATION

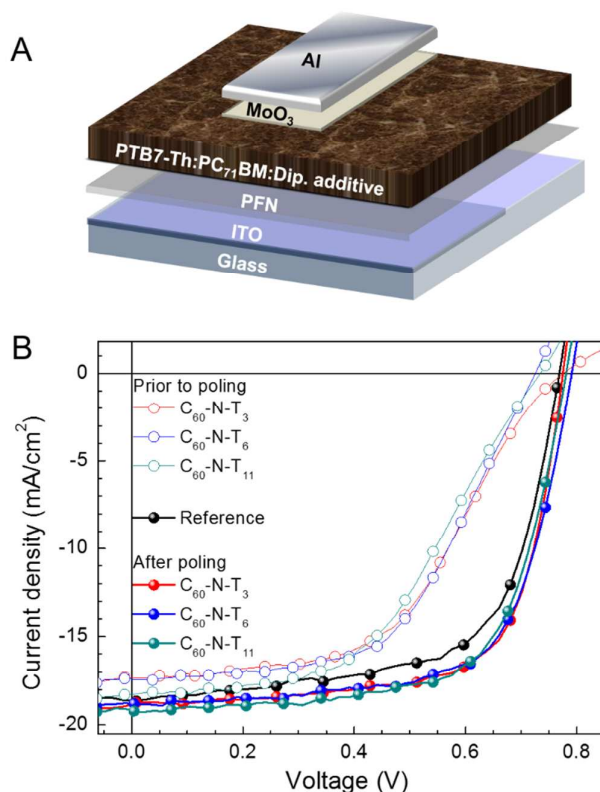
In an effort to increase the molecular dipole moment, two novel fulleropyrrolidine derivatives of  $C_{60}$ -N-T<sub>3</sub> were synthesized where the electron deficient fullerene core and electron rich tertiary amines were separated by longer tethers.<sup>13</sup> All three derivatives were synthesized in two facile steps from commercial starting materials. First, Mitsunobu coupling of 2,3,4-trihydroxybenzaldehyde and an amino-alkyl-alcohol containing 3, 6 or 11 methylene units in the alkyl chain, provided the amino-benzaldehyde intermediates, as shown in **Scheme 1**. Second, a Prato reaction between the amino-benzaldehyde intermediates, sarcosine, and fullene- $C_{60}$  yielded the desired fulleropyrrolidines,  $C_{60}$ -N-T<sub>3</sub>,  $C_{60}$ -N-T<sub>6</sub> and  $C_{60}$ -N-T<sub>11</sub>, corresponding to tethers with 3, 6, and 11 methylene units, respectively, separating the fulleropyrrolidine and tertiary amines (**Scheme 1**). Successful Prato reactions were indicated by a change in solution color from violet ( $C_{60}$ ) to brown, and confirmed using <sup>1</sup>H nuclear magnetic resonance (NMR) spectroscopy. The appearance of doublets at ~4.9 and 4.2 ppm are diagnostic of the geminal protons  $\alpha$  to the cyclic amine of the pyrrolidine product. Moreover, matrix-assisted laser desorption/ionization time-of-flight (MALDI-TOF) mass spectrometry of the products confirmed the identity of the three fulleropyrrolidines, providing  $m/z$  values of 1157.60, 1284.45, and 1494.47 for  $[M+H]^+$  molecular ions (details in the SI).



**Scheme 1.** Synthesis of  $C_{60}$ -N-T<sub>3</sub>,  $C_{60}$ -N-T<sub>6</sub>, and  $C_{60}$ -N-T<sub>11</sub> additives. (i) Diisopropyl azodicarboxylate, triphenylphosphine, 3-(dimethylamino)-X-1-ol, THF, 30-70%, where X corresponds to propan, hexan and undecan for  $C_{60}$ -N-T<sub>3</sub>,  $C_{60}$ -N-T<sub>6</sub> and  $C_{60}$ -N-T<sub>11</sub>, respectively; (ii) Fullerene- $C_{60}$ , sarcosine, chlorobenzene, 33-54%.

A schematic illustration of the inverted device configuration used in this study is provided in **Figure 1A**. Poly[4,8-bis(5-(2-ethylhexyl)thiophen-2-yl)benzo[1,2-b;4,5b']-dithiophene-2,6-diyl-*alt*-(4-(2-ethylhexyl)-3-fluorothiopheno[3,4-*b*]thiophene)-2-carboxylate-2,6-diyl)] (PTB7-Th) was the donor in the active layer and [6,6]-phenyl- $C_{71}$ -butyric acid methyl ester (PC<sub>71</sub>BM) was the acceptor component (chemical structures shown in the SI). The top and bottom contacts were a transparent indium tin oxide (ITO)/ poly[(9,9-bis(3'-(*N,N*-dimethylamino)propyl)-2,7-fluorene)-*alt*-2,7-(9,9-diocetylfluorene)] (PFN) cathode and molybdenum trioxide (MoO<sub>3</sub>) / aluminum (Al) anode. These were selected for their

favorable energy alignment for inverted device architectures, providing efficient extraction of photo-generated charge carriers.<sup>14</sup> The amount of dipolar additives in the active layer was optimized with regard to the device performance for  $C_{60}$ -N-T<sub>3</sub> additives (0.5 volume percent (v%)), as shown in Figure S1 and Table S1, and matching quantities (0.5 v%) were used for devices containing  $C_{60}$ -N-T<sub>6</sub> and  $C_{60}$ -N-T<sub>11</sub>. Figure 1B provides the J-V characteristics under simulated solar irradiation for the reference device (without dipolar additives) and devices with 0.5 v%  $C_{60}$ -N-T<sub>3</sub>,  $C_{60}$ -N-T<sub>6</sub>, and  $C_{60}$ -N-T<sub>11</sub> additives prior to poling (open symbols) and after poling



(-2 V, solid symbols).

**Figure 1.** Solar cell device schematic and performance. (A) Inverted solar cell architecture. (B) Current density-voltage characteristics with and without dipolar additives before (open symbols) and after (solid symbols) -2 V poling.

The key device performance parameters are summarized in **Table 1**. The reference devices show a maximum  $V_{OC} = 0.77$  V,  $J_{SC} = 18.4$  mA·cm<sup>-2</sup> and FF = 64.9%, providing a PCE ( $\eta$ ) = 9.2%. However, the reference devices deteriorate with electric-field poling, reaching a  $V_{OC} = 0.78$  V,  $J_{SC} = 16.0$  mA·cm<sup>-2</sup>, FF = 61.2% and  $\eta = 7.7\%$  after 20 min at -2 V. Notably, devices with dipolar additives have a reduced performance relative to the reference devices prior to poling (metrics given in **Figure S2** and **Table S3**). This result is similar to the observations made by Cao and coworkers for devices that contained amine-functionalized methanofullerenes (PC<sub>71</sub>BM-N) in the active layer, which was suggested to arise from hole trapping.<sup>12</sup> However, after poling at -2 V (forward diode direction), the

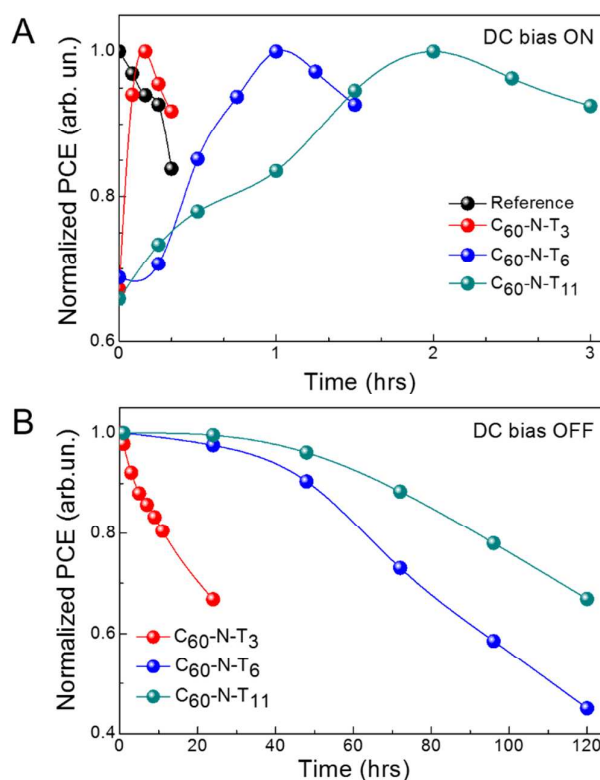
performance of devices containing dipolar additives improves by  $\sim 10\%$  compared to the reference devices (without dipolar additives), and  $>50\%$  compared to as-made (non-poled) devices containing dipolar additives, providing PCE values of  $\sim 10\%$  for all three amine-functionalized fulleropyrrolidines. Specifically, devices with  $C_{60}\text{-N-T}_3$  showed  $V_{OC} = 0.78$  V,  $J_{SC} = 18.9$   $\text{mA}\cdot\text{cm}^{-2}$ , FF = 69.1% and  $\eta = 10.1\%$ , while devices with  $C_{60}\text{-N-T}_6$  showed  $V_{OC} = 0.79$  V,  $J_{SC} = 18.8$   $\text{mA}\cdot\text{cm}^{-2}$ , FF = 67.8% and  $\eta = 10.1\%$  and devices with  $C_{60}\text{-N-T}_{11}$  showed  $V_{OC} = 0.78$  V,  $J_{SC} = 19.1$   $\text{mA}\cdot\text{cm}^{-2}$ , FF = 66.8% and  $\eta = 10.0\%$  (Table 1). Notably the enhanced FF and  $J_{SC}$  are largely responsible for the improvement of device performance, while the  $V_{OC}$  remains comparable for poled devices with respect to reference devices. This result highlights the generality of the approach given that the improvement in device performance as a result of electric-field poling is similar to behavior observed for small-molecule-based solar cell devices having a regular (non-inverted) device architecture with  $C_{60}\text{-N-T}_3$  additives.<sup>9</sup>

**Table 1.** Summary of device performance with and without (reference) electrochromic additives. Poling done at -2V with denoted time.

Sample	Poling (min)	$J_{SC}$ ( $\text{mA}\cdot\text{cm}^{-2}$ )	$V_{OC}$ (V)	FF (%)	$\eta$ (%) (average)
Reference	0	18.4	0.77	64.9	9.2 (9.0 $\pm$ 0.2)
Reference	20	16.0	0.78	61.2	7.7 (7.5 $\pm$ 0.2)
$C_{60}\text{-N-T}_3$	0	17.3	0.78	50.2	6.8 (6.4 $\pm$ 0.3)
$C_{60}\text{-N-T}_3$	10	18.9	0.78	69.1	10.1 (9.7 $\pm$ 0.4)
$C_{60}\text{-N-T}_6$	0	17.4	0.72	55.0	6.9 (6.7 $\pm$ 0.3)
$C_{60}\text{-N-T}_6$	60	18.8	0.79	67.8	10.1 (9.8 $\pm$ 0.3)
$C_{60}\text{-N-T}_{11}$	0	18.3	0.73	49.2	6.6 (6.2 $\pm$ 0.4)
$C_{60}\text{-N-T}_{11}$	120	19.1	0.78	66.8	10.0 (9.7 $\pm$ 0.3)

Interestingly, by systematically varying the tether length, temporal characteristics of poled electrochromic additives are significantly altered. Figure 2A shows the normalized PCE of devices with different additives for different durations of electric-field poling. The individual J-V characteristics of the devices are shown in Figure S2 and device performance parameters are summarized in Tables S2-S5. As stated previously, the PCE values for the reference devices decreased from 9.2 to 7.7% over the course of poling at -2V for 20 min., while in contrast, all devices containing dipolar additives show improved performance as a result of poling over time scales on the same order of magnitude. Prior to poling, devices with  $C_{60}\text{-N-T}_3$  had a PCE of 6.8% (6.4 $\pm$ 0.4%), which steadily improved over 10 min of poling at -2 V, reaching a maximum PCE of 10.1% (9.7 $\pm$ 0.4%) (Figure S2b, Table S3). Additional poling (+10 min), resulted in a PCE decrease to 9.3% (9.1 $\pm$ 0.2%) primarily due to a lower  $J_{SC} = 17.9$   $\text{mA}\cdot\text{cm}^{-2}$ . The peak performance highlights the balance between dipole orientation to improve performance and device degradation under continuous electrical stress. Similarly, devices with  $C_{60}\text{-N-T}_6$  (Figure S2c,

Table S4) and  $C_{60}\text{-N-T}_{11}$  (Figure S2d, Table S5) initially benefited from poling, although on different time scales;  $\eta = 6.9\%$  (6.7 $\pm$ 0.3%) to 10.1% (9.8 $\pm$ 0.3%) after 60 min of poling for devices with  $C_{60}\text{-N-T}_6$  and  $\eta = 6.2\%$  (6.7 $\pm$ 0.4%) to 10.0% (9.7 $\pm$ 0.3%) after 120 min of poling for devices with  $C_{60}\text{-N-T}_{11}$ . The devices degraded with extended poling, likely due to the trade-off between performance-enhancing orientation of dipoles and degradation under electrical stress. Therefore, it is anticipated that photovoltaic devices with enhanced stability could benefit further from the use of dipolar additives, since deleterious background degradation would be eliminated. External quantum efficiency (EQE) spectra of the corresponding devices are shown in Figure S3. For all devices, high and uniform EQE values were observed between 400-800 nm, suggesting efficient conversion of photons to free charge carriers throughout the visible region of the solar spectrum. For reference devices the EQE peaks at  $\sim 76\%$  around 700 nm, while nearly  $\sim 90\%$  EQE is observed for electrochromic devices at the same wavelength, which corresponds to the peak absorption of PTB7-Th. The improved EQE for devices



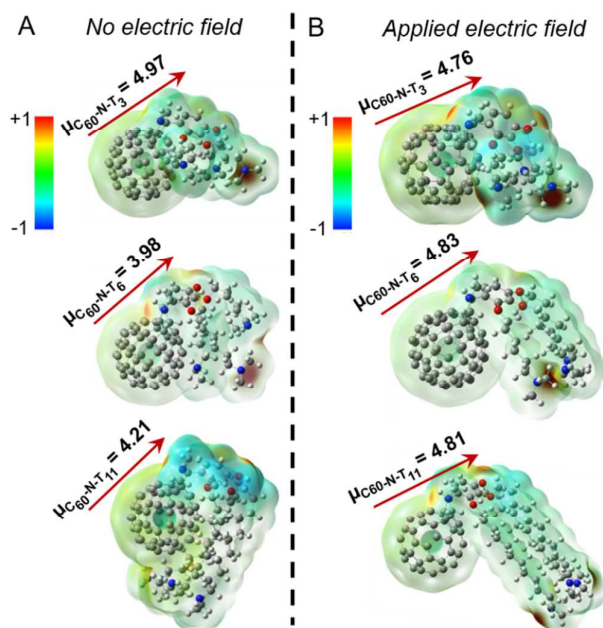
containing electrochromic additives as compared to the reference devices is consistent with the improved J-V characteristics.

**Figure 2.** Temporal characteristics of ferroelectric polarization. (A) Normalized power conversion efficiency of devices as a function of poling time, (B) Normalized power conversion efficiency of devices after poling (e.g., DC bias off).

Additional device improvement observed upon poling in the presence of electrochromic additives was the retention time

for the ferroelectric polarization. **Figure 2B** shows the normalized efficiency of devices with fulleropyrrolidine additives as a function of time after poling (e.g., DC bias off).  $C_{60}$ -N-T<sub>3</sub> based devices showed a quick dissolution of the effect, losing 30% efficiency within 24 hrs. Alternatively,  $C_{60}$ -N-T<sub>6</sub> and  $C_{60}$ -N-T<sub>11</sub> based devices showed prolonged stability, losing 30% of their initial efficiency after 72 and 120 hrs, respectively. It is interesting to note that the poling time required for achieving the highest efficiency of the current devices and their prolonged stability vary systematically with the additive molecules. To better understand the origin of the effect and explain temporal variations, density functional theory (DFT) calculations were undertaken.

The DFT calculations<sup>24,25</sup> probed molecular geometries, dipole moments, and electrostatic potential maps for the ground states of the fulleropyrrolidine additives, as shown in **Figure 3A**. The computed dipole moment for  $C_{60}$ -N-T<sub>3</sub> is 4.97 D, which originates from the lone pair electrons of the tertiary amines, as suggested by the electrostatic potential maps. The antiparallel position of the two amine groups may compensate each other, which results in a lower permanent dipole moment in the optimized structure. In contrast, the optimized structures of  $C_{60}$ -N-T<sub>6</sub> and  $C_{60}$ -N-T<sub>11</sub> show distinct interactions between the tertiary amine groups and the electron deficient fullerene core, allowed by the increased flexibility of the longer hydrocarbon-tethers, which reduces the dipole moments to 3.98 and 4.21 D, respectively. While the amine-fullerene interaction is apparent in the optimized structures, the electrostatic maps show no ground-state electron transfer (e.g., n-doping of fullerene), in agreement with the



photoexcitation shown to induce electron transfer in PC<sub>71</sub>BM in the presence of amines.<sup>26,27</sup> To investigate the effect of electric field on the structure and electrostatic properties of the molecules, an external field, with strength on

**Figure 3.** Molecular geometries with dipole moment vectors (left) and electrostatic potential maps (right) for electrootropic additives under no electric field (A) and under an external electric field (B).

the same order of magnitude as device poling ( $\sim 10^6$ - $10^7$  V/m), was applied to the calculation. The optimized structures and their corresponding electrostatic maps are shown in **Figure 3B**, revealing dramatic structural changes as the tertiary amines extend away from the fullerene core. This extension causes an increase of dipole moments for  $C_{60}$ -N-T<sub>6</sub> and  $C_{60}$ -N-T<sub>11</sub> to approximately 4.8 D, which is comparable with  $C_{60}$ -N-T<sub>3</sub> and is consistent with the nearly identical peak PCE values obtained for all poled devices. Moreover, larger conformational changes for derivatives with longer side chains correlates with the requirement for increased poling and retention times. It is speculated that local Joule heating that occurs in response to the flow of electrical current during poling can be used to explain the relatively rapid chain alignment during poling in comparison to the observed relaxation post-poling, where the side-chains are effectively “frozen” in the surrounding matrix. Therefore, synthesizing additive molecules with large dipole moments that are distributed over long side chains may further improve device efficiency and stability.

## Conclusions

In summary, the synthesis, device integration and computational analysis of three amine-functionalized fulleropyrrolidine derivatives,  $C_{60}$ -T-N<sub>3</sub>,  $C_{60}$ -T-N<sub>6</sub> and  $C_{60}$ -T-N<sub>11</sub>, were reported. Extending the tether length between the electron rich amines and deficient fullerene core led to systematic variations in poling times necessary to reach peak device power conversion efficiencies and ferroelectric polarization retention times. Combining photovoltaic device performance analysis with DFT calculations revealed underlying structure-property relationships between the newly developed electrootropic molecules and photophysics associated with electrical field poling. Of significance, the longer tether groups led to significantly improved retention times of ferroelectric polarization in the inverted photovoltaic devices, reaching PCE values in excess of 10%. This study opens new prospects for energy harvesting by developing high-efficiency solution processable OPV devices using dipolar additives and electric field poling to enhance performance.

## Acknowledgements

Supported by the Polymer-Based Materials for Harvesting Solar Energy (PHaSE), an Energy Frontier Research Center funded by the U.S. Department of Energy (DOE), Office of Basic Energy Sciences, under award DE-SC0001087. We thank PHaSE and the NSF-MRSEC on Polymers at UMass (DMR-0820506) for facilities support.

## Notes and references

- 1 J. U. Lee, J. W. Jung, T. Emrick, T. P. Russell and W. H. Jo, *J. Mater. Chem.*, 2010, **20**, 3287–3294.
- 2 B. K. Sivula, Z. T. Ball, N. Watanabe and J. M. J. Fréchet, *Adv. Mater.*, 2006, **18**, 206–210.
- 3 C. Yang, K. Lee, J. Heeger and F. Wudl, *J. Mater. Chem.*, 2009, **19**, 5416–5423.
- 4 H. Fujita, T. Michinobu, S. Fukuta, T. Koganezawa and T. Higashihara, *ACS Appl. Mater. Interfaces*, 2016, **8**, 5484–5492.
- 5 F. Lombeck, A. Sepe, R. Thomann, R. H. Friend and M. Sommer, *ACS Nano*, 2016, **10**, 8087–8096.
- 6 K. R. Graham, P. M. Wieruszewski, R. Stalder, M. J. Hartel, J. Mei, F. So and J. R. Reynolds, *Adv. Funct. Mater.*, 2012, **22**, 4801–4813.
- 7 H. Jhuo, S. Liao, Y. Li, P. Yeh, S. Chen, W. Wu, C. Su, J. Lee, N. L. Yamada and U. Jeng, *Adv. Funct. Mater.*, 2016, **26**, 3094–3104.
- 8 J. K. Lee, W. L. Ma, C. J. Brabec, J. Yuen, J. S. Moon, J. Y. Kim, K. Lee, G. C. Bazan and A. J. Heeger, *J. Am. Chem. Soc.*, 2008, **130**, 3619–3623.
- 9 S. Karak, Z. A. Page, J. S. Tinkham, P. M. Lahti, T. Emrick and V. V. Duzhko, *Appl. Phys. Lett.*, 2015, **106**.
- 10 Z. He, C. Zhong, S. Su, M. Xu, H. Wu and Y. Cao, *Nat. Photonics*, 2012, **6**, 591–595.
- 11 Y. Zhou, C. Fuentes-Hernandez, J. Shim, J. Meyer, A. J. Giordano, H. Li, P. Winget, T. Papadopoulos, H. Cheun, J. Kim, M. Fenoll, A. Dindar, W. Haske, E. Najafabadi, T. M. Khan, H. Sojoudi, S. Barlow, S. Graham, J.-L. Brédas, S. R. Marder, A. Kahn and B. Kippelen, *Science*, 2012, **336**, 327–332.
- 12 C. Duan, W. Cai, B. B. Y. Hsu, C. Zhong, K. Zhang, C. Liu, Z. Hu, F. Huang, G. C. Bazan, A. J. Heeger and Y. Cao, *Energy Environ. Sci.*, 2013, **6**, 3022–3034.
- 13 Z. A. Page, Y. Liu, V. V. Duzhko, T. P. Russell, T. Emrick, *Science* 2014, **346**, 441.
- 14 Y. Liu, Z. A. Page, T. P. Russell and T. Emrick, *Angew. Chemie - Int. Ed.*, 2015, **54**, 11485–11489.
- 15 B. Russ, M. J. Robb, F. G. Brunetti, P. L. Miller, E. E. Perry, S. N. Patel, V. Ho, W. B. Chang, J. J. Urban, M. L. Chabiny, C. J. Hawker and R. A. Segalman, *Adv. Mater.*, 2014, **26**, 3473–3477.
- 16 F. Liu, Z. A. Page, V. V. Duzhko, T. P. Russell and T. Emrick, *Adv. Mater.*, 2013, **25**, 6868–6873.
- 17 C. Sun, Z. Wu, H. L. Yip, H. Zhang, X. F. Jiang, Q. Xue, Z. Hu, Z. Hu, Y. Shen, M. Wang, F. Huang and Y. Cao, *Adv. Energy Mater.*, 2016, **6**, 1501534.
- 18 T. Y. Juang, J. C. Kao, J. C. Wang, S. Y. Hsu, C. P. Chen, *Adv. Mat. Int.* 2018, **5** (10), 1800031.
- 19 B. H. Jiang, Y. J. Peng and C. P. Chen, *J. Mater. Chem. A*, 2017, **5**, 10424.
- 20 Z. Xiao, Q. Dong, P. Sharma, Y. Yuan, B. Mao, W. Tian, A. Gruverman, and J. Huang, *Adv. Energy Mater.* 2013, **3**, 1581.
- 21 K. S. Nalwa, J. A. Carr, R. C. Mahadevapuram, H. K. Kodali, S. Bose, Y. Chen, J. W. Petrich, B. Ganapathysubramanian and S. Chaudhary, *Energy Environ. Sci.*, 2012, **5**, 7042.
- 22 Z. Xiao, Q. Dong, Q. Wang, W. Tian, H. Huang, and J. Huang, *IEEE Journal of photovoltaics*, 2015, 5(5), 1408.
- 23 S. Fabiano, S. Braun, X. Liu, E. Weverberghs, P. Gerbaux, M. Fahlman, M. Berggren and X. Crispin, *Adv. Mater.*, 2014, **26**, 6000–6006.
- 24 A. D. Becke, *J. Chem. Phys.*, 1993, **98**, 5648.
- 25 A. D. Becke, *Phys. Rev. A*, 1988, **38**, 3098–3100.
- 26 L. Nian, W. Zhang, N. Zhu, L. Liu, Z. Xie, H. Wu, F. Würthner and Y. Ma, *J. Am. Chem. Soc.*, 2015, **137**, 6995–6998.
- 27 Z. Wu, C. Sun, S. Dong, X. F. Jiang, S. Wu, H. Wu, H. L. Yip, F. Huang and Y. Cao, *J. Am. Chem. Soc.*, 2016, **138**, 2004–2013.

## TOC Graphic

